Core-cusp problem in equivalent Newtonian systems of MOND $N-$body simulations

Federico Re[1,2] **& Pierfrancesco Di Cintio**[3,4,5]

[1]Dipartimento di Fisica "Giuseppe Occhialini", Universitá di Milano Bicocca, Piazza della Scienza 3 20126, Milano, Italy
[2]INFN-Sezione di Milano Via Celoria 15 20133, Milano, Italy; [3] CNR-ISC, via Madonna del Piano 17 50022 Sesto Fiorentino, Italy;
[4]INFN-Sezione di Firenze, via Sansone 1 50022 Sesto Fiorentino, Italy; [5]INAF-Osservatorio Astronomico di Arcetri, Largo Enrico Fermi 5 50125 Firenze Italy

The core-cusp problem

In the ΛCDM scenario, theoretical arguments and collisionless $N-$body simulations predict that galaxies are embedded in dark matter (DM) halos characterized by a $\rho(r) \propto r^{-1}$ central cusp [13]. Observational results seem to suggest, from the analysis of the central velocity dispersion profiles of dwarf galaxies, that the DM distribution has a cored density distribution [11, 5].
Several solutions to this (apparent) contradiction, such as self-interacting DM [6], baryon feedback [14] or simply a misinterpretation of the observational data [7], have been proposed so far. In this preparatory work we investigate this matter further in the modified Newtonian dynamics (MOND) paradigm, in the context of the so called equivalent Newtonian systems (ENS).

Modified Newtonian dynamics

In the Bekenstein & Milgorm formulation [1] of MOND [8] the Poisson equation

$$\Delta\Phi = 4\pi G\rho \tag{1}$$

is substituted by the non-linear field equation

$$\nabla\cdot\left[\mu\left(\frac{||\nabla\Phi||}{a_0}\right)\nabla\Phi\right] = 4\pi G\rho, \tag{2}$$

where $a_0 \approx 10^{-8}\mathrm{cm\ s}^{-2}$ is a scale acceleration and the interpolating function $\mu(x)$ is known only in its asymptotic limits

$$\mu(x) \rightarrow^{x\gg 1} 1, \quad \mu(x) \sim^{x\ll 1} x, \tag{3}$$

so that for $||\nabla\Phi|| \gg a_0$ Eq. (2) is in the Newtonian regime, while for $||\nabla\Phi|| \ll a_0$ one recovers essentially the so-called deep-MOND regime and Eq. (2) simplifies to the

$$\nabla\cdot[||\nabla\Phi||\nabla\Phi] = 4\pi G\rho a_0. \tag{4}$$

Note that, in both cases, any given baryonic mass density ρ can be taken out from the classical Poisson equation (1) obtaining the relation

$$\mu\left(\frac{||\mathbf{g}_M||}{a_0}\right)\mathbf{g}_M = \mathbf{g}_N + \mathbf{S} \tag{5}$$

between the MOND and Newtonian force fields $\mathbf{g}_M$ and $\mathbf{g}_N$, and where $\mathbf{S} \equiv \nabla\times\mathbf{h}(\rho)$ is a density-dependent solenoidal field. It can be proved that the latter is identically null for systems in spherical, cylindrical or planar symmetry, while it is generally non-zero for arbitrary configurations of mass.
For a given system in MOND, one can always define a model in Newtonian gravity with the same baryon density (and velocity distribution) and and additional "DM halo" such that the total potential is the same of the MOND model. We now discuss the concept of equivalent Newtonian system.

Structure of equivalent Newtonian systems

At any instant, it can be considered the potential Φ generated by a distribution ρ_B of baryonic mass, according the MOND law (2). The same potential Φ is justified in the ENS by a total density $\rho_N := \rho_B + \rho_{DM}$, according to the Newtonian law (1). Under the simplifying assumption of spherical symmetry, the density ρ_N in the ENS is related to ρ_B as

$$\rho_M(r) = \left[\mu(x)) + x\mu'(x))\right]\rho_N(r) - \frac{2}{r}\mu(x)\int_0^r \rho_N(r)dr. \tag{6}$$

In the centre, the argument $x = ||\nabla\Phi(r)||/a_0$ tends to zero if the baryons have a flat core, or even if they have a weak enough cusp, i.e. $\rho_B(r) \sim \rho_{B0}(r_s/r)^\alpha$ with $\alpha < 1$. For such a case, it holds the deep MOND asymptotic $\mu(x) \sim x$ in the centre, and the formula (6) returns

$$\rho_N(r) \sim \frac{5-\alpha}{4}\sqrt{\frac{a_0\rho_{B0}r_s^\alpha}{\pi(3-\alpha)G}}\cdot r^{-\frac{1+\alpha}{2}}. \tag{7}$$

This means for the DM a weaker cusp $\rho_{DM}(r) \propto r^{-\frac{1+\alpha}{2}} < r^{-1}$ than the one emerging from the simulations.
In particular, for a flat baryon density, one has

$$\rho_{DM}(r) \sim \frac{5}{4}\sqrt{\frac{a_0\rho_{B0}}{3\pi G}}\cdot r^{-1/2}. \tag{8}$$

The associated gravitational acceleration becomes

$$g(r) = ||\nabla\Phi(r)|| \sim \sqrt{\frac{4}{3}\pi G a_0\rho_{B0}}\cdot r^{1/2}, \tag{9}$$

while the velocity for circular stable orbits is

$$v_{circ}(r) \sim \sqrt[4]{\frac{4}{3}\pi G a_0\rho_{B0}}\cdot r^{3/4}, \tag{10}$$

that one could compare with empirical velocity profiles.

Structure of equivalent Newtonian systems

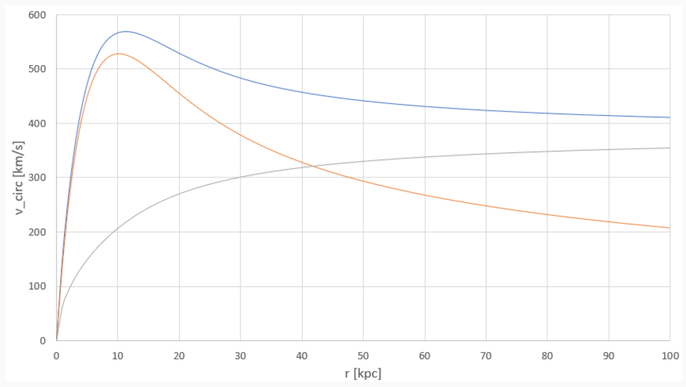

In the figures, are shown the rotation curves $v_{circ}(r)$ and the cumulative masses $M(r) = \int_0^r 4\pi r^2\rho(r)dr$ for an exponential baryon distribution $\rho_B(r) := \rho_{B0}e^{r/r_s}$, with scalar radius of $r_s := 3$ kpc and total mass of 10^{12} solar masses. The blue lines refers to the total mass ρ_N in the ENS, while the red lines correspond to the baryon component only, and the grey lines to the DM one.

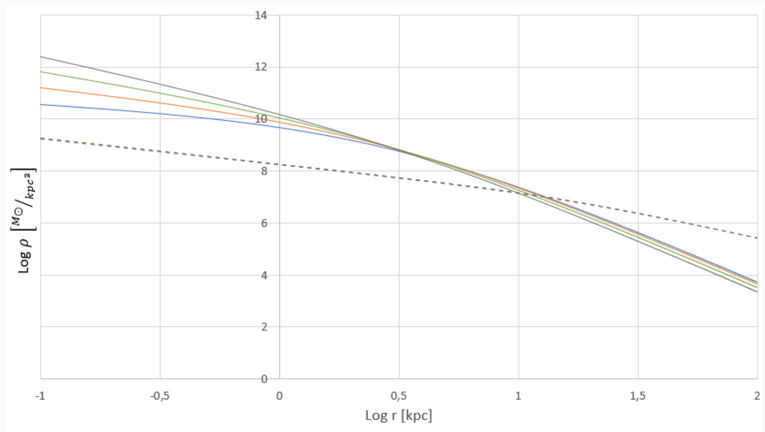

Other examples are given in this figure, for the so called $\gamma-$models [4], defined by the density profile

$$\rho_B(r) = \frac{3-\gamma}{4\pi}\frac{Mr_c}{r^\gamma(r+r_c)^{4-\gamma}}, \tag{11}$$

with total mass $M := 10^{12}M_\odot$, scale radius $r_c := 3$ kpc and logarithmic density slope $\gamma := 0.5$ in blue, $\gamma := 1$ in red, $\gamma := 1.5$ in green, and $\gamma := 2$ in grey. Solid lines represent the baryonic densities, while the dashed lines (which are approximately overlapping) plot the DM densities, in log-log scale.

Numerical Simulations

Code and initial conditions

The $N-$body simulations discussed here have been performed with a modified version of the publicly available NMODY particle-mesh MOND code (see [12]). The latter uses a non-linear Poisson solver to compute Φ from Eq. (2) on a spherical grid in polar coordinates. We assumed the following forms for the interpolation function

$$\mu_1(x) = \frac{x}{\sqrt{1+x^2}}; \quad \mu_2(x) = \frac{x}{1+x}. \tag{12}$$

Our simulations span a range of N between 10^4 and 10^6. As a rule, the simulations were extended up to $t = 300t_{\mathrm{Dyn}}$, where $t_{\mathrm{Dyn}} \equiv \sqrt{2r_h^3/GM_{\mathrm{tot}}}$ and r_h is the radius containing half of the total mass of the system M_{tot}.
The positions for the particles of the $i-$th component (baryonic or DM) in spherical systems were sampled from the family of $\gamma-$models, with density profile given by Eq. (11).
Initial particle velocities are extracted from a position-independent Maxwell-Boltzmann distribution and normalized to obtain the wanted value of the initial virial ratio $2K/|W|$.
Following [3] we enforce the spherical symmetry by propagating particles only using the radial part of the evaluated force field, so that the system behaves effectively as a spherical shell model [15]. For each simulation we recover the (spherical) phantom DM density as

$$\rho_{DM} = (4\pi G)^{-1}\nabla\cdot(\mathbf{g}_M - \mathbf{g}_N) \tag{13}$$

where the Newtonian force field g_N has been evaluated and averaged on the radial coordinate.

Numerical Simulations

Simulations and results

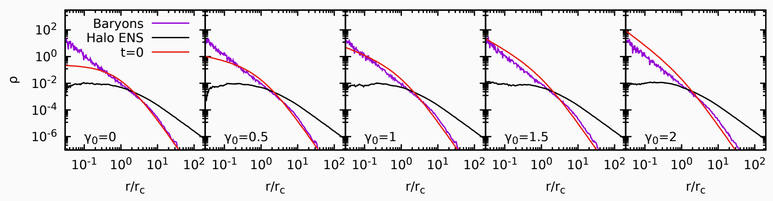

In the figure above we show the final density profile ($t = 300t_{\mathrm{Dyn}}$) of purely radial collapses (purple lines) and that of the phantom DM of the ENS (black lines, evaluated using Eq. 13) for systems starting from cold ($2K/W = 0$) $\gamma-$model initial conditions (red lines).
In all cases ($\gamma = 0$, 0.5, 1, 1.5 and 2), even if the mass density relaxes to a rather cuspy distribution, the parent ENS has a flat DM halo.

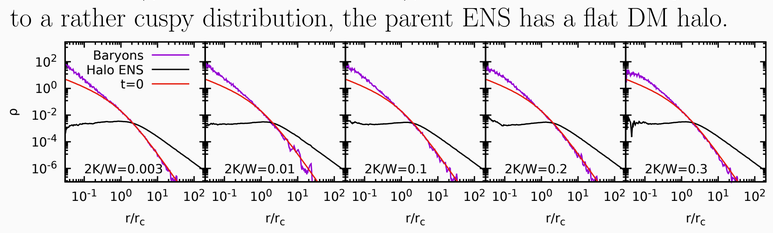

Above we show the final states of collapses starting with initial conditions characterized by a moderate cusp ($\gamma = 1$) and $3\times10^3 \le 2K/|W| \le 0.3$. In this cases we observe that (at least) for colder initial conditions and warm, the DM in the ENS has a cored density profile. Remarkably, for intermediate values of the initial virial ratio, the halo of the ENS presents several slope changes at small radii. For both sets of simulations, the results are qualitatively unchanged independently on the choice of μ.

Conclusions and perspectives

The preliminary results of this work can be summarized as follows:

- Analytical estimates suggest that the presence of a flat core in the DM distribution embedding a spheroidal galaxy as evidenced by some observational studies, can be interpreted in the context of MOND as purely the effect of the phantom DM having a week cusp, independently on the specific value of the central logarithmic density slope of the baryons. Remarkably, a week cusp can be oftem mistaken for a core.
- The end product of simplified MOND $N-$body simulation with enforced spherical symmetry have ENS with markedly flat cores, for a broad spectrum of initial values of density slope and virial ratio, despite the fact that the baryon density always has is rather cuspy at inner radii.

As mentioned above, the simulation presented here are rather unrealistic in their nature, in particular due to the imposed spherical symmetry. Other numerical experiments with full MOND force and clumpy initial conditions are on the way. In that case, one can not evaluate the DM density in the simple spherical approximation using Eq. (13), but could instead use the so-called Quasi-linear formulation of MOND (QuMOND) [9] where one first evaluates the Newtonian field $\mathbf{g}_N$ Eq. 1 and then uses it as the source density term for the phantom halo potential after applying the algebraic step

$$\tilde{\rho}_{DM} = -(4\pi G)^{-1}\nabla\cdot[\nu(g_N/a_0)\mathbf{g}_N], \tag{14}$$

where $\nu(x)$ is the reciprocal of the previously defined MOND interpolating function $\mu(y)$.

References

[1] Bekenstein, J.; Milgrom, M. *ApJ* **286**, 7 (1984)
[2] Binney, J.; Tremaine, S. Galactic dynamics 2nd edition, Princeton University Press NJ (2008)
[3] Ciotti, L.; Nipoti, C.; Londrillo, P. Proceedings of the International Workshop "Collective Phenomena in Macroscopic Systems", G. Bertin, R. Pozzoli, M. Rome, and K.R. Sreenivasan, eds., World Scientific, Singapore, pp.177-186 (2007)
[4] Dehnen, W., *MNRAS* **265**, 250D (1993)
[5] Di Cintio, A.; Brook, Ch. B.; Macciò, A. V. et al., *MNRAS* **437**, 414 (2014)
[6] Lovell, M. *MNRAS* **420**, 2318 (2012)
[7] McGaugh S. S., Barker M. K., de Blok W. J. G., *ApJ* **584**, 566 (2003)
[8] Milgrom, M. *ApJ* **270**, 365 (1983)
[9] Milgrom, M. *MNRAS* **403**, 886M (2010)
[10] Milgrom, M.; Sanders, R. H., *ApJ* **678**, 131 (2008)
[11] Moore, B. *Nature* **370**, 629 (1994)
[12] Nipoti, C.; Londrillo, P.; Ciotti, L. *ApJ* **660**, 256 (2007)
[13] Navarro, J. F.; Frenk, C. S.; White, S. D. M. *ApJ* **490**, 493 (1997)
[14] Pontzen, A. *Nature* **421**, 3464 (2012)
[15] Sanders, R. H. MNRAS **386**, 1588 (2008)